N_2–Kr interaction: A multiproperty analysis

Frederick R. W. McCourt
Departments of Chemistry and Physics, University of Waterloo, Waterloo N2L 3G1, Canada

Marc A. ter Horst[a] and Cynthia J. Jameson
Department of Chemistry M/C-111, University of Illinois at Chicago, 845 West Taylor Street, Chicago, Illinois 60607-7061

(Received 21 October 1994; accepted 6 January 1995)

An earlier anisotropic N_2–Kr potential energy surface [Chem. Phys. Lett. **88**, 197 (1982)] of Lennard-Jones form, obtained by inversion of molecular beam differential scattering data, has been found to provide calculated transport–relaxation phenomena in good agreement with experiment, but leads to calculated second interaction virial coefficients which are significantly too low, and does not provide adequate agreement with recent microwave van der Waals spectral data. A modification of this surface to include a recent *ab initio* determination of the C_6 dispersion coefficient, and to bring in the virial and microwave data, gives a new potential surface that is in good agreement with all available experimental data. © *1995 American Institute of Physics.*

I. INTRODUCTION

Much has been learned about the anisotropic nature of intermolecular interactions from studies involving the interaction of a closed shell diatomic molecule with a closed shell atom. Interactions between the hydrogen isotopomers and noble gas atoms were the first to be studied in detail, for the obvious reasons that large amounts of experimental data, both spectroscopic and nonspectroscopic, are available, they are amenable to *ab initio* calculations, and exact scattering calculations are relatively easy to carry out for them. Some determinations of these interactions treated the hydrogen molecule as a rigid rotor,[1–3] while others have included a dependence upon the stretching motion of the hydrogen molecule.[4–6]

Nonspectroscopic data, such as molecular beam scattering and bulk virial, transport, and relaxation data have been found to be very useful for determination of parameters characterizing the repulsive part of the interaction potentials, together with the position and depth of the potential minimum, but are not generally very useful in providing details of the potential well and the parameters characterizing the attractive part of the interaction potential. Spectroscopic data, by contrast, have proven to be extremely useful in characterizing these latter features, and less useful in characterizing the former. Of course, determination of the potential well also represents an indirect determination of the repulsion energy, since the features of the well represent a compromise between the repulsive and attractive components of the overall interaction. The most accurate determination of the full interaction potential surface will result from a multiproperty analysis, in which both types of data, as well as *ab initio* theoretical results, are utilized.

Although the hydrogen isotopomers serve in many ways as prototypical linear molecules, they have the disadvantage of producing only weakly anisotropic interactions, with the consequence that hydrogenic interactions are not sufficiently representative of anisotropic interactions to allow fully general conclusions to be drawn from their study. The interactions between HF and HCl molecules and noble gas atoms provide more prototypical anisotropic interactions, and they have been studied intensively recently[7] because of the wealth of spectroscopic data available for these two molecules in various environments. The disadvantage for employing the hydrogen halide–rare gas interactions as prototypical interactions is that molecular beam, spectroscopic, bulk virial, transport, and relaxation data are generally not all available.

A set of molecular interactions for which there are now available not only beam scattering data,[8–10] bulk virial,[11] transport,[12,13] and relaxation data,[14–16] but more recently also spectroscopic data associated with van der Waals complexes,[17–19] are those between nitrogen and the noble gases. Indeed, the interactions between N_2 and He, Ne, Ar have been extensively studied during the past four or five years,[20–23] and can now be considered to be quite well characterized. The same cannot yet be said, however, for the interactions of N_2 with Kr and Xe.

Specific properties which are utilized in multiproperty determinations of intermolecular interaction potentials for unlike species are: second interaction virial coefficients, diffusion coefficients, mixture shear viscosity and thermal conductivity coefficients, external field effects[24] on the transport coefficients (or Senftleben–Beenakker effects), collision broadening and shifting of infrared and/or Raman spectral lines of the constituent molecules, collision broadening of the depolarized Rayleigh line, nuclear magnetic relaxation times at the bulk (or macroscopic) level, and molecular beam scattering and the infrared and/or microwave spectra of the van der Waals complexes at the microscopic level. Measurements of the first four properties, together with the total differential and integral scattering cross-section measurements, have often been employed to establish a reasonably refined isotropic component of the interaction potential surface, together with first estimates of the anisotropy of the well position and well depth. The microwave spectrum of the van der Waals complex can then be used to fine tune the position of the minimum,[25] while rotational state-to-state differential

[a]Present address: Department of Chemistry, Northwestern University, Evanston, IL 60208-3113.

 0021-9606/95/102(14)/5752/9/$6.00

cross sections (if available), the external field effects on the transport phenomena and nuclear magnetic relaxation times can be utilized to fine tune the anisotropy on the repulsive wall and at the potential minimum. The infrared spectrum of the van der Waals complex and the collision broadening and shifting of the spectroscopic lines can then be used to check the overall potential.

We shall present a newly determined simple anisotropic potential for the N_2–Kr interaction that provides good agreement between its predictions and all available measured properties of N_2–Kr mixtures, both spectroscopic and nonspectroscopic.

II. FORM OF THE POTENTIAL ENERGY FUNCTION

An anisotropic Lennard-Jones (12,6) potential function was determined by Rotzoll[8] from total differential cross-section measurements at a collision energy of 80.77 meV. He utilized the form recommended by Pack[26] to represent the anisotropy through the potential parameters R_m and ϵ characterizing the position and depth of the potential minimum as a function of the relative orientation of one collision partner to the other. Thus, if the angle between the directions $\hat{\mathbf{u}}$ of the N_2 figure axis and $\hat{\mathbf{R}}$ of the line joining the centers of mass of the N_2 molecule and the Kr atom is designated by γ, then the Rotzoll Lennard-Jones (12,6) potential function is given by

$$V(R,\gamma)=\epsilon(\gamma)\left[\left(\frac{R_m(\gamma)}{R}\right)^{12}-2\left(\frac{R_m(\gamma)}{R}\right)^{6}\right], \tag{1}$$

with $\epsilon(\gamma)$, $R_m(\gamma)$ given by

$$\epsilon(\gamma)=\epsilon_0[1+a_2P_2(\cos\ \gamma)], \tag{2a}$$

$$R_m(\gamma)=R_{m0}[1+b_2P_2(\cos\ \gamma)]. \tag{2b}$$

Rotzoll determined best-fit potential parameter values $\epsilon_0=516.1\ \mu$h (micro-hartrees), $R_{m0}=7.558\ 91\ a_0$ (bohrs), $a_2=-0.25$, $b_2=0.09$.

To our knowledge, until recently this was the only anisotropic full potential function for the N_2–Kr interaction in the literature. It is based solely upon a fitting of the parameters ϵ_0, R_{m0}, a_2, b_2 to molecular beam scattering data at a single collision energy, and is, as such, an empirical potential, necessarily of the simplest kind. A more sophisticated description of the repulsive part of the N_2–Kr interaction energy, based upon *ab initio* self-consistent field Hartree–Fock (SCF-HF) calculations, has been given by Nyeland and Toennies,[27] while there have been several recent *ab initio* calculations of the long-range dispersion energy[28] at the SCF-configuration-interaction level. Various versions of more sophisticated models for the interaction potential, often referred to as the HFD (from Hartree–Fock plus damped dispersion)[29(a)] or the TT (for Tang–Toennies)[29(b)] model potential, have been constructed recently.[30,31] Perhaps surprisingly, none of these more sophisticated determinations has given a potential energy function which agrees with available experimental data as well as does the fully empirical Rotzoll potential.[31] Indeed, the main weakness of the Rotzoll potential is that it does not give acceptable agreement with the temperature dependence of the second interaction virial coefficient, largely due to an overestimation of the well-depth parameter ϵ_0.

Quite recently microwave (MW) spectra of the N_2–Kr van der Waals complex have become available.[19] It has also been established recently[25] that the positions of the centers of gravity of the experimentally observed MW hyperfine transitions provide a sensitive probe of $R_m(\gamma)$. Thus, since a calculation of the centers of gravity of the MW lines associated with the N_2–Kr complex based upon the original Rotzoll potential surface already gives considerably better agreement with the MW data than do calculations based upon the other model surfaces mentioned above, it was decided to modify the Rotzoll potential surface to bring the calculated temperature dependence of the interaction second virial coefficient and the MW spectrum of the van der Waals complex into agreement with experiment. To make the new potential energy surface somewhat more realistic, it was also decided to modify the long-range dispersion component so as to incorporate the recent accurate determination[28] of the C_6 dispersion coefficient; all remaining uncertainty is then buried, in principle, into the empirical C_8 coefficient.

The new Lennard-Jones (12,6,8) potential function can hence be written in the form

$$V(R,\gamma)=\bar{C}_{12}(\gamma)\left(\frac{R_m}{R}\right)^{12}-\frac{C_6(\gamma)}{R^6}-\frac{C_8(\gamma)}{R^8} \tag{3a}$$

$$=\bar{C}_{12}(\gamma)\left(\frac{R_m}{R}\right)^{12}-\bar{C}_6(\gamma)\left(\frac{R_m}{R}\right)^{6}-\bar{C}_8(\gamma)\left(\frac{R_m}{R}\right)^{8}, \tag{3b}$$

with $R_m\equiv R_m(\gamma)$ given by Eq. (2b), and $C_6(\gamma)$, $C_8(\gamma)$ given by

$$\begin{aligned} C_6(\gamma)&=C_6^{(0)}+C_6^{(2)}P_2(\cos\ \gamma),\\ C_8(\gamma)&=C_8^{(0)}+C_8^{(2)}P_2(\cos\ \gamma)+C_8^{(4)}P_4(\cos\ \gamma). \end{aligned} \tag{4}$$

The $\bar{C}_n$ in Eqs. (3) represent reduced coefficients, related to the corresponding $C_n(\gamma)$ via $\bar{C}_n(\gamma)=C_n(\gamma)/[R_m(\gamma)]^n$. We note also that $\bar{C}_{12}(\gamma)$ is not an independent parameter in the potential, and is related to $\bar{C}_6(\gamma)$ and $\bar{C}_8(\gamma)$ by

$$\bar{C}_{12}(\gamma)=\tfrac{1}{2}\bar{C}_6(\gamma)+\tfrac{2}{3}\bar{C}_8(\gamma). \tag{5}$$

Similarly, $\epsilon(\gamma)$ can be related to $\bar{C}_6(\gamma)$ and $\bar{C}_8(\gamma)$ by

$$\epsilon(\gamma)=\tfrac{1}{2}\bar{C}_6+\tfrac{1}{3}\bar{C}_8(\gamma). \tag{6}$$

Finally, since it is often convenient to work in terms of $\bar{R}_m(\gamma)$ and $\epsilon(\gamma)$, it is possible, using Eq. (6), to express $C_8(\gamma)$ in terms of $C_6(\gamma)$ and $\epsilon(\gamma)$, so that the independent parameters determining the overall potential are those appearing in $R_m(\gamma)$ and $\epsilon(\gamma)$, recalling that $C_6(\gamma)$ has been fixed at the *ab initio* values given in Ref. 28. This is the approach that has been taken here.

Molecular beam total differential scattering data are more sensitive to R_m than to ϵ, and appear typically to be able to determine R_{m0} to within $\pm1\%$, ϵ_0 to within $\pm5\%$, but the anisotropy parameters a,b are determined only to within $\pm20\%$.[23] Reasonable agreement with the second interaction virial data (±2 cm^3/mol for $T<200$ K, ±1 cm^3/mol for $T>200$ K) could not be achieved within these limitations,

TABLE I. Parameters for the LJ(12,6,8) N_2–Kr potential surface.

Parameter	N_2–Kr
$\epsilon_0/\mu h$	485.1
R_{m0}/a_0	7.630 905
a_2	−0.300
b_2	0.0900
$C_6^{(0)}/a_0^6 h$	94.4
$C_6^{(2)}/a_0^6 h$	8.2189

and it was necessary to decrease ϵ_0 by 6% in order to obtain agreement that could still be considered to be reasonable. We thus recommend $\epsilon_0 = 485.1$ μh (cf. Rotzoll value 516.1 μh). With this value for ϵ_0 a best fit to the MW spectral data (see Sec. III) gives $R_{m0} = 7.630\,905$ a_0 (cf. Rotzoll value 7.558 91 a_0). The angular dependence of the long-range C_6 coefficient was determined [see Eq. (4)] according to the *ab initio* values $C_6^{(0)} = 94.4h$ a_0^6 and $C_6^{(2)} = 8.2189h$ a_0^6 given by Hettema *et al.*[28] for the N_2 equilibrium separation $r_{N_2} = 2.068$ a_0. Note that although the value of r_{N_2} differs from the value $r_{N_2} = 2.079$ a_0 for N_2 in its $v=0$ ground vibrational state, the (small) differences that would arise due to changes in the values of $C_6^{(0)}$ and $C_6^{(2)}$ are subsumed in the resultant value taken by the $C_8(\gamma)$ coefficients. A complete set of relevant parameters for the Lennard-Jones (12,6,8) potential is given in Table I. The two potential surfaces are compared in Fig. 1, showing cuts at 0° and 90°.

III. COMPARISON BETWEEN CALCULATED AND MEASURED PROPERTIES

A comparison between the temperature dependence of the second interaction virial coefficient in the range $145\ \text{K} \leqslant T \leqslant 350\ \text{K}$ is shown in Table II. The calculations have been carried out using the semiclassical method, including first radial and angular quantum corrections, for both the original Rotzoll LJ(12,6) potential and the modified LJ(12,6,8) potential. The experimental values are those of Brewer.[32] As mentioned in Sec. II, the values of $B_{12}(T)$ calculated from the original Rotzoll potential strongly disagree

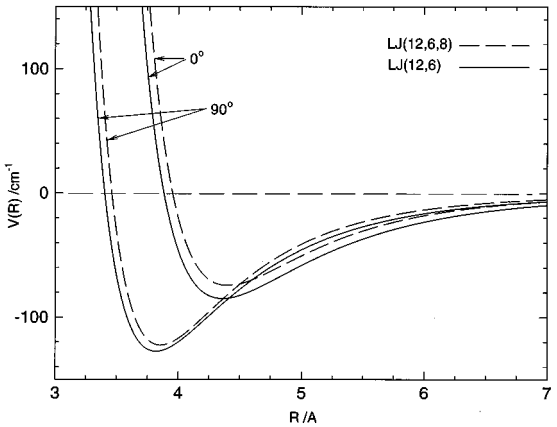

FIG. 1. Cuts of the LJ(12,6) and LJ(12,6,8) potential energy surfaces for the collinear (0°) and perpendicular (90°) approaches of Kr to N_2.

TABLE II. Temperature dependence of the interaction second virial coefficient for N_2–Kr mixtures.

	$B_{12}(T)/\text{cm}^3\,\text{mol}^{-1}$		
T/K	LJ(12,6)	LJ(12,6,8)	Expt.[a]
148.15	−168.2	−124.7	−119.6
173.15	−128.0	−92.24	−89.14
198.15	−100.44	−69.86	−67.92
223.15	−80.34	−53.56	−52.68
273.1	−53.10	−31.47	−30.71
323.1	−35.57	−17.27	−17.08

[a]Experimental data have been taken from Ref. 32.

with experiment. Those calculated using the modified LJ(12,6,8) potential are in good agreement with experiment, i.e., within ±1 cm^3/mol error bars for temperatures in excess of 200 K. Note that while it would likely be possible to bring the calculated values within ±1 cm^3/mol error bars at all temperatures, it would require us to reduce the parameter ϵ_0 to a value well outside that allowed by the molecular beam data; we have chosen to select a value of ϵ_0 that lies just outside the lower limit consistent with the beam data, and which still gives values of B_{12} that can be considered to be in good agreement with the experimental values.

The energy levels for the N_2–Kr van der Waals complex were calculated using the TRIATOM suite of programs developed by Tennyson *et al.*[33] The calculations were at the same level of accuracy as those for N_2–Ar described in detail in Ref. 25. At the fitting stage the only $J'' \rightarrow J'$ MW transitions utilized were those corresponding to $(J'',J') = (1,2)$ and (2,3) for each of the $\Sigma^e(0)$, $\Pi^f(1)$, $\Pi^e(1)$ sequences of pure rotational lines for the $^{14}N_2$–^{86}Kr van der Waals complex. The original Rotzoll LJ(12,6) potential surface gave line positions for this van der Waals complex that differed from the experimentally observed $\Sigma^e(0)$, $\Pi^f(1)$, $\Pi^e(1)$ lines by 1.76%, 1.64%, and 1.95%, respectively; this indicated that R_{m0} was not very far from its optimal value. By increasing R_{m0} by 0.95%, to 7.630 905 a_0, the calculated MW line positions were brought to within better than 0.27% of the experimental positions in all three sequences. No further improvement is possible within the confines of the LJ(12,6,8) potential form and reasonable computational effort. A comparison between calculated and observed MW transition frequencies is given in Table III.

The LJ(12,8,6) potential surface, as determined from beam scattering, virial coefficient, and MW data, was then tested against the temperature dependence of the bulk gas transport and relaxation data available for N_2–Kr mixtures. Classical trajectory (CT) calculations for the N_2–Kr interaction were carried out for a full set of effective cross sections (see Refs. 24,34) relevant to the bulk gas phenomena.

Meaningful comparison with transport data requires not only highly accurate experimental data (i.e., data with small random errors and essentially free from systematic errors) but also accurately calculated effective cross sections and sufficiently complete theoretical expressions that the calculated values of the transport properties are converged to well within the overall experimental errors. The experimental ac-

TABLE III. Comparison of experimental center frequencies of N_2–Kr complexes with those calculated from the LJ(12,6,8) potential energy surface.[a]

Isotopomer	Sequence	$J''-J'$	ν_{calc} /MHz	ν_{obs} /MHz	δ_ν/ν_{obs} /%
$^{14}N_2$–^{86}Kr	$\Sigma^e(0)$	1–2	6 000.92	6 000.9548	−0.005
		2–3	9 000.09	8 999.8657	+0.002
		3–4	11 997.69	11 996.9031	+0.007
		4–5	14 993.22	14 991.4253	+0.012
	$\Pi^f(1)$	1–2	6 047.33	6 056.3765	−0.144
		2–3	9 069.73	9 083.0636	−0.147
		3–4	12 090.59	12 107.9429	−0.143
		4–5	15 109.42	15 130.4267	−0.139
	$\Pi^e(1)$	1–2	5 934.29	5 918.6803	+0.264
		2–3	8 900.17	8 876.3364	+0.268
		3–4	11 864.51	11 831.9659	+0.275
		4–5	14 826.81	14 784.8860	+0.284
$^{14}N_2$–^{84}Kr	$\Sigma^e(0)$	1–2	6 035.16	6 035.2692	−0.002
		2–3	9 051.42	9 051.3218	+0.001
		3–4	12 066.11	12 065.4734	+0.005
		4–5	15 078.68	15 077.0816	+0.011
	$\Pi^f(1)$	1–2	6 082.05	6 091.2154	−0.150
		2–3	9 121.79	9 135.3039	−0.148
		3–4	12 159.98	12 177.5679	−0.144
		4–5	15 196.11	15 217.3941	−0.140
	$\Pi^e(1)$	1–2	5 967.70	5 951.8899	+0.266
		2–3	8 950.26	8 976.1294	+0.270
		3–4	11 936.28	11 898.3187	+0.272
		4–5	14 910.22	14 867.7641	+0.286
$^{15}N_2$–^{86}Kr	$\Sigma^e(0)$	1–2	5 709.11	5 710.3496	−0.022
		2–3	8 562.50	8 564.1205	−0.019
		3–4	11 414.49	11 416.2061	−0.015
		4–5	14 264.60	14 266.0383	−0.010
	$\Pi^f(1)$	1–2	5 753.36	5 761.9633	−0.149
		2–3	8 628.90	8 641.5875	−0.147
		3–4	11 503.06	11 519.5936	−0.143
		4–5	14 375.40	13 295.4332	−0.139
	$\Pi^e(1)$	1–2	5 646.01	5 632.5051	+0.240
		2–3	8 467.87	8 447.2557	+0.244
		3–4	11 288.37	11 260.2104	+0.250
		4–5	14 107.05	14 070.7529	+0.258
$^{15}N_2$–^{84}Kr	$\Sigma^e(0)$	1–2	5 743.40	5 744.7311	−0.023
		2–3	8 613.92	8 615.6757	−0.020
		3–4	11 483.02	11 484.9131	−0.016
		4–5	14 350.22	14 351.8673	−0.001
	$\Pi^f(1)$	1–2	5 788.15	5 796.8646	−0.150
		2–3	8 681.01	8 693.9284	−0.148
		3–4	11 572.59	11 589.3514	−0.146
		4–5	14 462.27	14 482.5787	−0.140
	$\Pi^e(1)$	1–2	5 679.48	5 665.7982	+0.242
		2–3	8 518.08	8 497.1807	+0.246
		3–4	11 355.28	11 326.7428	+0.252
		4–5	14 190.64	14 153.8658	+0.260
$^{15}N_2$–^{82}Kr	$\Sigma^e(0)$	1–2	5 779.34	5 780.7616	−0.025
		2–3	8 667.81	8 669.7044	−0.022
		3–4	11 554.84	11 556.9150	−0.018
	$\Pi^f(1)$	1–2	5 824.61	5 833.4513	−0.152
		2–3	8 735.74	8 748.7863	−0.149
		3–4	11 645.46	11 662.4604	−0.146
		4–5	14 553.31	14 573.9117	−0.141
	$\Pi^e(1)$	1–2	5 714.56	5 700.6881	+0.243
		2–3	8 570.68	8 549.4896	+0.248
		3–4	11 425.39	11 396.4498	−0.254
		4–5	14 278.23	14 240.9372	+0.262
$^{14}N^{15}N$–^{86}Kr	$\Sigma^e(0)$	2–3	8 773.98	8 774.9277	−0.011
		3–4	11 696.34	11 697.1354	−0.007
		4–5	14 616.72	14 616.9624	−0.002
$^{14}N^{15}N$–^{84}Kr	$\Sigma^e(0)$	2–3	8 825.36	8 826.4347	−0.012
		3–4	11 764.82	11 765.7774	−0.012
		4–5	14 702.27	14 702.7124	−0.003

[a]Experimental values are from Ref. 19.

curacies reported for the diffusion, shear viscosity, and thermal conductivity measurements that are to be used for comparison with the present calculations are all of the order of ±0.5% or better: we shall treat these values as optimal uncertainties. To obtain calculations that lie within such stringent limits it is necessary to utilize a higher kinetic theory approximation for the transport phenomena than the first Chapman–Cowling approximation[24] normally employed for the analysis of such data. The present calculations will thus require second approximation Chapman–Cowling corrections to be made. These correction factors may be calculated from the isotropic components of the appropriate potential surfaces, since they are typically of the order of 0.2%–0.8%, and the relevant effective cross sections required for their calculation are determined largely by the isotropic components of the potential surfaces (to >96%). Very little relative error is introduced by such a procedure. Further, at this level of comparison it will also be useful to include, insofar as possible, angular momentum polarization effects[24] associated with the polyatomic component. The second Chapman–Cowling approximation corrections are all positive, while the angular momentum polarization contributions to the transport coefficients are also typically positive, as can be deduced from the normal decrease in the values of the transport coefficients when a magnetic field is applied to the bulk gas. The polarization correction should be applied first, after which the second Chapman–Cowling correction should be made. This is a nontrivial procedure for binary mixtures.

Four sets of diffusion data are available for N_2–Kr mixtures. The most recent direct measurements are those of Trengove and Dunlop,[35] covering the temperature range 280 K≤T≤340 K, and of Wahby,[36] covering the temperature range 200 K≤T≤440 K. In addition Hellemans *et al.*[12] have extracted diffusion coefficients from their mixture shear viscosity data, and Marrero and Mason[37] have compiled earlier directly measured values of the diffusion coefficients and produced a smoothed correlation from them. The anisotropic nature of the intermolecular interactions involving polyatomic molecules introduces nonequilibrium angular momentum polarizations in a nonequilibrium gas, and these polarizations make small contributions to the transport coefficients.[24] Their magnitudes are indicated by the size of the changes in the transport coefficients when a magnetic field is applied: although they contribute typically less than 1% to the total transport coefficient, they are in many instances competitive with second approximation corrections to the transport coefficients. Polarization contributions to the diffusion coefficient are known to be smaller than are those to the shear viscosity and thermal conductivity coefficients.[24] Calculations of the polarization corrections for the N_2–Kr diffusion coefficient indicate that they are of the order of 0.07%, so that they can be neglected in the present analysis. Second Chapman–Cowling corrections for the diffusion coefficient are considerably larger for this interaction, of the order of 1%, so that they must be considered in a detailed comparison between calculations of the present accuracy and experiment.

The binary diffusion coefficient is independent of mole fraction in the first Chapman–Cowling approximation, de-

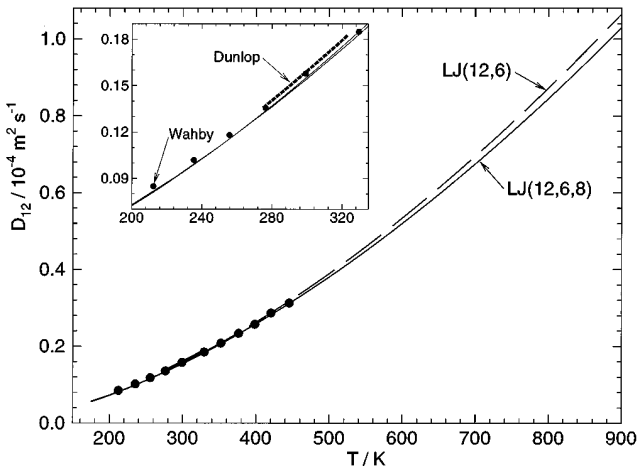

FIG. 2. Comparison of the temperature dependence of the binary diffusion coefficient for N_2–Kr mixtures. The solid and dashed curves represent, respectively, the first Chapman–Cowling approximation calculations for the LJ(12,6,8) and LJ(12,6) potential energy surfaces, while the experimental points are those of Wahby (Ref. 36, solid circles), Trengove and Dunlop (Ref. 35, heavy dashed line). The inset shows the comparison at lower temperatures in greater detail.

noted here by $[D]_1$, but depends upon the mole fraction in the second, denoted here by $[D]_2(x_A)$, and higher Chapman–Cowling approximations.[38] A comparison between the experimental values for the diffusion coefficient and diffusion coefficients obtained from first Chapman–Cowling approximation calculations based upon CT values for the diffusion cross section is shown in Fig. 2. The solid curve represents the diffusion coefficient calculated with the present LJ(12,6,8) potential surface, and the dashed curve represents the diffusion coefficient calculated with the original Rotzoll LJ(12,6) potential surface. In both cases agreement with experiment can be considered to be acceptable over the entire range of temperature. However, as can be seen from the more detailed comparison for $x_{N_2} = 0.50$ given in Table IV, the diffusion coefficients calculated from both potentials are smaller than the direct measurements of Trengove and Dunlop[35] by nearly 2%, and lower than those deduced by Hellemans *et al.*[12] from their shear viscosity data by nearly 1%. The percentage differences, δ, reported in this and the following tables are given by (calculated value − experimental value)×100% divided by the experimental value. They are in considerably better agreement with the direct measurements reported by Wahby[36] and with the earlier correlated data of Marrero and Mason.[37] The diffusion coefficients calculated from the original Rotzoll potential surface are generally in better agreement with the data of Trengove and Dunlop[35] and Hellemans *et al.*[12] than are those obtained from the modified LJ(12,6,8) potential surface, but they are in poorer agreement with the data of Wahby[36] and of Marrero and Mason[37] than are those calculated from the LJ(12,6,8) potential surface. At the temperatures at which the absolute measurements of the diffusion coefficients were measured (300.0 K for Trengove and Dunlop, 299.16 K for Wahby) the two directly determined experimental diffusion coefficients differ by about 2.8%, so that these two experimental determinations do not overlap within their stated uncertainties (assumed for Wahby to be ±0.5%).

A comparison between the measured mixture viscosity η_{mix} for N_2–Kr binary mixtures and that calculated via the first Chapman–Cowling approximation, with CT values for the relevant N_2–Kr effective cross sections as input, is shown in Fig. 3 for temperatures 298, 467, and 767 K. As usual, experimental values of η for $x_{N_2} = 0,1$ are employed, so that meaningful comparison can only be made for values of $x_{N_2} \neq 0,1$. The shear viscosity for pure N_2 has been corrected for polarization effects and for the second Chapman–Cowling approximation contribution prior to the effective cross section being obtained by inversion of the experimental data; the shear viscosity for pure Kr has similarly been corrected for the second Chapman–Cowling contribution prior to inversion. The dashed curves correspond to the original Rotzoll LJ(12,6) surface, while the solid curves correspond to the LJ(12,6,8) surface reported here. The polarization corrections for the binary mixtures are larger than those for the diffusion coefficient, being of the order of 0.2%; such corrections have been applied in Table V via the relation $\eta_{\mathrm{mix}}(\mathrm{iso}) = \eta_{\mathrm{mix}}(\mathrm{measured})/f_{02\eta}$. Here η_{mix}(iso) refers to the mixture shear viscosity for an ''isotropic'' distribution function, i.e., a nonequilibrium distribution function which does not depend upon the direction of the rotational angular momentum vector **j**. Second Chapman–Cowling approximation correction factors $f_{2\eta}$ for the mixture are also larger than for diffusion, and are of the order of 0.2%–0.6%; they slightly improve the agreement between the values calculated from the LJ(12,6,8) surface and experiment, as can be seen from Table V, though the agreement is still not fully quantitative. These corrections do, however, bring the viscosities calculated from the original Rotzoll LJ(12,6) potential surface into quantitative agreement with experiment.

Calculation of the thermal conductivity coefficient for a polyatomic gas or for a binary mixture containing a polyatomic gas is inherently more complicated than is the calculation of either the diffusion or shear viscosity coefficients, because molecules possess both translational and internal rotational (and vibrational) energy that can be transported through the nonequilibrium gas. As a result, the calculation of the thermal conductivity coefficient for a polyatomic gas requires, in lowest approximation, three independent effective cross sections, rather than only one. Further, calculations of the thermal conductivity of binary mixtures require in addition to the set of the three effective cross sections determined by the unlike molecule interaction, also the corresponding effective cross sections associated with the pure gas interactions.

In the present case this requires three effective cross sections for the unlike N_2–Kr interaction, three cross sections for the N_2–N_2 interaction, and one cross section for the Kr–Kr interaction. The cross sections for the N_2–Kr interaction have been obtained from CT calculations with both the present LJ(12,6,8) potential surface and the original LJ(12,6) potential surface of Rotzoll. The cross section needed for Kr at the level of a first Chapman–Cowling approximation can either be calculated directly from the appropriate potential

TABLE IV. Temperature dependence of the diffusion coefficient for N_2–Kr binary mixtures for $x_{Kr}=0.50$ (units: 10^{-4} m^2 s^{-1}).[a]

T/K	$[D]_1$	$[D]_2(0.50)$	δ/%	$D(0.50)$	D_{expt}
212.28	0.0816	0.0826	−2.71	0.0849	0.0850[b]
	0.0811	0.0820	−3.42		
235.42	0.0990	0.1003	−1.57	0.1019	0.1020[b]
	0.0988	0.1001	−1.77		
255.72	0.1154	0.1169	−0.85	0.1179	0.1182[b]
	0.1156	0.1171	−0.68		
276.44	0.1331	0.1349	−0.37	0.1354	0.1356[b]
	0.1325	0.1355	0.07		
298.15	0.1528	0.155	−0.64,1.31	0.156,0.153	0.156[c],0.153[d]
	0.1540	0.156	0.00,1.96		
299.16	0.1545	0.1566	0.26	0.1562	0.1580[b]
	0.1557	0.1578	1.02		
300.0	0.1545	0.1566	−2.06	0.1599	0.1595[e]
	0.1557	0.1578	−1.31		
320.0	0.1735	0.1759	−2.17	0.1798	0.1794[e]
	0.1753	0.1777	−1.20		
329.53	0.1829	0.1854	0.54	0.1844	0.1851[b]
	0.1849	0.1875	1.68		
352.36	0.2061	0.2090	0.87	0.2072	0.2083[b]
	0.2088	0.2117	2.17		
373.15	0.2282	0.231	−1.28,1.76	0.234,0.227	0.234[c],0.227[d]
	0.2314	0.235	0.43,3.52		
420.34	0.2813	0.2853	0.21	0.2847	0.2870[b]
	0.2865	0.2906	2.07		
473.15	0.3455	0.351	−1.68,1.44	0.357,0.346	0.357[c],0.346[d]
	0.3529	0.358	0.28,3.47		
573.15	0.4813	0.488	−2.01,0.62	0.498,0.485	0.498[c],0.485[d]
	0.4932	0.500	0.40,3.09		
673.15	0.6319	0.641	−2.43,−0.62	0.657,0.645	0.657[c],0.645[d]
	0.6505	0.660	0.46,2.33		
773.15	0.7985	0.811	−2.64,−1.46	0.833,0.823	0.833[c],0.823[d]
	0.8240	0.837	0.48,1.70		

[a]The upper entries for the first approximation, $[D]_1$, and for the second approximation, $[D]_2(x_A)$, at each temperature have been calculated from the modified LJ(12,6,8) potential, while the corresponding lower entries have been calculated from the original LJ(12,6) potential of Rotzoll (Ref. 8). At temperatures 298.15, 373.15, 473.15–773.15 K, there are two sources of diffusion coefficients, namely Refs. 12 and 37: values from these references appear side by side; pairs of values in the column marked δ give the corresponding percentage differences between calculation and experiment.
[b]Reference 36.
[c]Reference 12.
[d]Reference 37.
[e]Reference 35.

function,[39] or obtained by inversion of the experimental thermal conductivity once the second approximation correction factor $f_{2\lambda}$(Kr), calculated from the appropriate potential function has been applied. The latter procedure has been used in the present analysis. The appropriate effective cross sections for pure N_2 are much more difficult to obtain, since all existing literature values have been extracted from experimental data using analyses based upon first Chapman–Cowling approximation expressions, without angular momentum polarization corrections. These cross sections are too inaccurate to employ for a detailed comparison between theory and experiment. We have hence chosen to utilize recent accurate CT calculations carried out by Heck and Dickinson[40] from the N_2–N_2 potential surface of van der Avoird *et al.*[41] The present comparison employs both polarization and second Chapman–Cowling approximation correction factors. The polarization correction factor for pure N_2 has been calculated from effective cross sections supplied by Heck and Dickinson[40] to be $f_{12\lambda}=1.0068$, while those for the binary mixture have been obtained from the present CT calculations, and are given in Table VI. The polarization factors are applied to the experimental data to give $\lambda_{mix}(0)$. Second approximation correction factors are obtained in all cases from an appropriate isotropic potential (for the reasons given earlier). Correction factors calculated from the isotropic component of the potential of Ref. 41 agree almost quantitatively with those obtained by Heck *et al.*[42] using CT results obtained from the full potential surface. The second approximation correction factors $f_{2\lambda}$(mix) for the N_2–Kr interaction have been obtained from the isotropic-parameter limit potential; they are quite significant, of the order of 1%. Experimental measurements of the thermal conductivity for N_2–Kr mixtures have been made by Fleeter *et al.*[13] Their results, corrected for angular momentum polarization contributions, are compared with second Chapman–Cowling approximation calculations of the mixture thermal conductivity

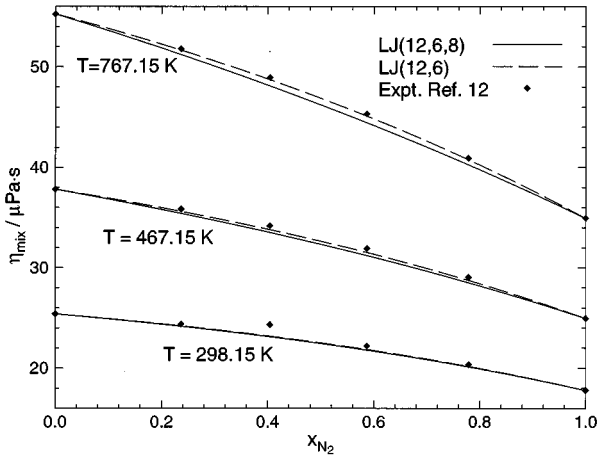

FIG. 3. Comparison for three temperatures between viscosities for N_2–Kr mixtures calculated from the LJ(12,6,8) (solid curve) and LJ(12,6) (dashed curve) potential energy surfaces using the first Chapman–Cowling approximation expression for η_{mix} and the experimental results of Hellemans *et al.* (Ref. 12).

in Table VI. As can be seen, the first approximation calculations, $[\lambda_{mix}]_1$, are in quite good agreement with the experimental results; the second-approximation corrections cause the final calculations to overshoot the experimental values by about 0.5% on average for the LJ(12,6,8) potential surface and by about 3.1% on average for the LJ(12,6) potential surface. These differences are well outside the experimental errors of $\pm 0.3\%$. This property is thus the least well described by both potential functions.

The temperature dependence of the NMR longitudinal relaxation time T_1 has been shown to provide a sensitive probe of the anisotropic nature of intermolecular interaction potentials.[24,23,43] In order to provide additional experimental data for use in refining the anisotropies of the potential surface, NMR data were acquired[15,16] both for $^{14}N_2$ and $^{15}N_2$ mixtures with a series of buffer gases. Since the nuclear spin of ^{14}N is 1, while the nuclear spin of ^{15}N is $\frac{1}{2}$, relaxation of the macroscopic nuclear magnetization in bulk $^{14}N_2$ and its mixtures can be caused by the collisional modulation of intramolecular spin–rotation, dipolar, and quadrupolar interactions, while that in bulk $^{15}N_2$ and its mixtures is caused by collisional modulation of the intramolecular spin–rotation and dipolar interactions. It happens that the quadrupolar interaction for $^{14}N_2$ is so much stronger than are the corresponding spin–rotation and dipolar interactions that the entire relaxation can be attributed to the quadrupolar relaxation in pure $^{14}N_2$ and its binary mixtures. Similarly, the dipolar interaction in $^{15}N_2$ is very much weaker than the spin–rotation interaction, so that only spin–rotation relaxation is monitored in pure $^{15}N_2$ and its binary mixtures. Consequently, measurements for these two isotopomeric species provide two independent sources of information on the anisotropic components of the intermolecular interaction potential. The effective cross sections relevant for these relaxation mechanisms are[24] $\mathfrak{S}(0100|A)_{AB}$, for the spin–rotation mechanism, and $\mathfrak{S}(0\hat{2}00|A)_{AB}$, for the quadrupolar mechanism, in which A represents N_2 and B represents Kr (or, more generally, the buffer species). For convenience we shall refer to these cross sections as NMR effective cross sections.

TABLE V. Comparison between calculated and experimental mole fraction dependence of the mixture viscosity for N_2–Kr binary mixture (units: μPa s).[a]

		Calculations			Experiment		
T/K	x_{N_2}	$[\eta_{mix}]_1$	$[\eta_{mix}]_2$	δ/%	η_{mix}(iso)	$f_{02\eta}$	η_{mix} (expt.)[b]
298.15	0.2363	24.049	24.186	−0.76	24.371	1.000 39	24.380
		24.092	24.230	−0.58			
	0.4041	23.035	23.153	−1.07	23.403	1.000 73	23.420
		23.099	23.217	−0.79			
	0.5866	21.725	21.829	−1.17	22.088	1.001 18	22.114
		21.795	21.899	−0.86			
	0.7786	20.062	20.155	−0.87	20.331	1.001 78	20.367
		20.117	20.211	−0.49			
367.15	0.2363	29.041	29.213	−0.62	29.396	1.000 37	29.407
		29.079	29.351	−0.15			
	0.4041	27.674	27.824	−0.95	28.092	1.000 73	28.113
		27.728	27.878	−0.76			
	0.5866	25.944	26.078	−1.07	26.360	1.001 17	26.391
		26.004	26.138	−0.84			
	0.7786	23.795	23.922	−0.80	24.114	1.001 76	24.156
		23.843	23.969	−0.60			
467.15	0.2363	35.233	35.447	−0.98	35.827	1.000 37	35.840
		35.431	35.646	−0.51			
	0.4041	33.371	33.557	−1.71	34.142	1.000 70	34.166
		33.654	33.843	−0.88			
	0.5866	31.099	31.270	−1.93	31.884	1.001 13	31.920
		31.408	31.581	−0.95			
	0.7786	28.388	28.553	−1.52	28.996	1.001 71	29.046
		28.626	28.793	−0.70			
571.15	0.2363	41.112	41.364	−1.25	41.886	1.000 36	41.901
		41.397	41.651	−0.56			
	0.4041	38.808	39.029	−1.72	39.713	1.000 67	39.740
		39.215	39.438	−0.69			
	0.5866	36.036	36.240	−1.86	36.927	1.001 10	36.968
		36.477	36.683	−0.66			
	0.7786	32.775	32.974	−1.40	33.443	1.001 66	33.499
		33.113	33.315	−0.38			
673.15	0.2363	46.370	46.657	−0.83	47.046	1.000 35	47.062
		46.734	47.023	−0.05			
	0.4041	43.670	43.992	−1.50	44.592	1.000 65	44.621
		46.734	47.023	−0.05			
	0.5866	40.440	40.673	−1.67	41.362	1.001 06	41.406
		40.998	41.234	−0.31			
	0.7786	36.666	36.894	−1.40	37.418	1.001 62	37.479
		37.094	37.325	−0.25			
767.15	0.2363	50.950	51.060	−1.35	51.758	1.000 34	51.776
		51.381	51.695	−0.12			
	0.4041	47.898	48.172	−1.50	48.905	1.000 64	48.936
		48.510	48.787	−0.24			
	0.5866	44.271	44.524	−1.67	45.278	1.001 04	45.325
		44.931	45.187	−0.20			
	0.7786	40.063	40.313	−1.34	40.861	1.001 59	40.926
		40.567	40.820	−0.10			

[a]The upper entries for $[\eta_{mix}]_1$ and $[\eta_{mix}]_2$ at each mole fraction have been calculated from the modified LJ(12,6,8) potential, while the lower entries have been calculated from the original Rotzoll LJ(12,6) potential (Ref. 8).
[b]Reference 12.

Comparison between calculated and experimental values for the NMR cross sections is shown in Fig. 4. It can be seen that the LJ(12,6,8) potential surface has a slightly greater anisotropy than does the original LJ(12,6) potential surface

TABLE VI. Comparison between calculated and experimental mole fraction dependence of the mixture thermal conductivity for N_2–Kr binary mixtures at 300.65 K (units: mW m^{-1} K^{-1}).[a]

	CT calculations			Experiment		
x_{N_2}	$[\lambda_{mix}]_1$	$[\lambda_{mix}]_2$	δ/%	λ_{mix}(iso)	$f_{12\lambda}$	λ_{mix}(expt.)[b]
0.4778	15.414	15.537	−0.40	15.594	1.014	15.812
	15.611	15.736	0.90	15.596	1.014	15.812
0.7054	19.315	19.62	1.40	19.35	1.023	19.80
	19.493	19.80	4.71	18.91	1.023	19.35

[a]The upper entries for $[\lambda_{mix}]_1$ and $[\lambda_{mix}]_2$ at each mole fraction have been calculated from the modified LJ(12,6,8) potential, while the corresponding lower entries have been calculated from the original LJ(12,6) potential of Rotzoll (Ref. 8).
[b]Reference 13.

of Rotzoll, since it gives rise to slightly larger values for both NMR effective cross sections. Both potential surfaces provide good agreement with the experimentally determined cross-section values, the Rotzoll surface giving slightly better agreement than does the LJ(12,6,8) surface.

IV. DISCUSSION AND CONCLUSIONS

We have seen in the previous section that the modified Lennard-Jones potential, designated LJ(12,6,8) and given by Eqs. (3) and (4), together with the parameter values appearing in Table I, gives accurately calculated bulk gas and microscopic properties that are in good agreement with all available experimental results for N_2–Kr mixtures. Minor modifications to the LJ(12,6) anisotropic potential surface originally determined by Rotzoll[8] from molecular beam scattering data alone results in the LJ(12,6,8) potential surface presented here. The set of data examined, while extensive, did not require a more sophisticated representation of the potential surface in order to achieve overall good agreement between calculations and experiment. However, it is almost certain that additional improvement in agreement with the experimental data is unlikely to be obtained with the present potential form, since it has been ''known'' for many years that the classic LJ(12,6) potential does not represent the interaction potential accurately even for noble gas atoms.[38,44] In particular the R^{-12} repulsive wall of the Lennard-Jones potential is too hard, and does not represent the ''true'' modified exponential (or Born–Mayer) behavior of the (essentially electronic) repulsion between two interacting species.

It has been shown conclusively[38,44] that no set of parameters for a LJ(n,m) potential can reproduce (i.e., within the most stringent experimental uncertainties available) the most accurate experimental values of all transport coefficients and spectral properties of the noble gases over an extended temperature range. This, taken together with the more intimate knowledge available today from *ab initio* quantum calculations of the interaction energy between two molecular species, has led to the development of ever more complicated representations of potential energy surfaces.[45] Given the above comments, one might well ask why it is that a LJ(12,6) or LJ(12,6,8) potential form is even being considered in the first place. Although this is, in principle, not an unreasonable question to ask, it is readily answerable: one uses the simplest representation for a potential surface that will provide acceptable agreement between the most accurate available calculations and experimental results. It is nonetheless surprising that a LJ-type potential surface appears to represent the interaction between N_2 and Kr so well.

It may be worth noting that although the direct modifications made to the LJ(12,6) potential form were made exclusively to the long-range component of the potential, these changes have also affected the short-range behavior in an indirect way, in that the repulsive wall of the LJ(12,6,8) potential is slightly harder than that of the original LJ(12,6) potential. This can be seen by comparing the net repulsive energy for the two potentials for distances shorter than σ, the distance at which the potential energy vanishes. This increased hardness of the LJ(12,6,8) potential is manifested in slightly larger transport cross-section values, and consequently slightly smaller transport coefficients, as can be seen from Figs. 2 and 3 and Tables IV and V. A comparison of cuts of the two potential surfaces at 90° and 0° (see Fig. 1) shows that the anisotropy in the position of the potential minimum is slightly larger for the LJ(12,6,8) potential surface (by about 0.1%) than for the LJ(12,6) surface, and that the anisotropy in the depth of the potential minimum is larger for the LJ(12,6,8) potential surface by about 12.8%. Both increased potential anisotropy and increased hardness of the repulsive wall affects the relaxation cross sections in much the same way: this is evident from Fig. 4, since the dipolar relaxation cross-section $\mathfrak{S}(0\hat{2}00|A)_{AB}$ is mostly sensitive to the potential anisotropy, while the spin–rotation relaxation cross-section $\mathfrak{S}(0100|A)_{AB}$ senses both potential anisotropy and changes in the repulsive wall of the potential similarly.

Calculations of second interaction virial coefficients, the centers of gravity of the hyperfine structure microwave lines of the N_2–Kr van der Waals complex, transport coefficients, and NMR longitudinal relaxation times based upon a potential surface obtained by a slight extension and modification

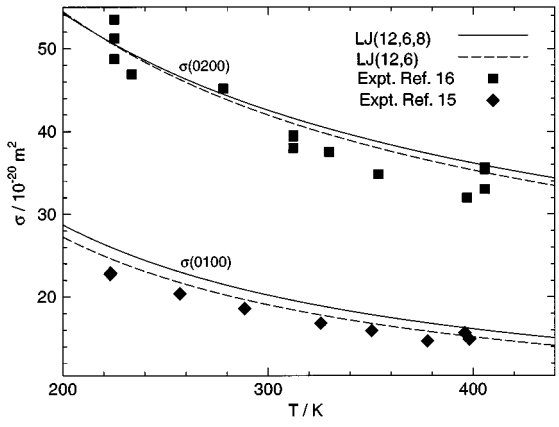

FIG. 4. The temperature dependence of the NMR relaxation cross-sections $\mathfrak{S}(0\hat{2}00|A)_{AB}$, governing relaxation of the nuclear spin magnetization of $^{14}N_2$, and $\mathfrak{S}(0100|A)_{AB}$, governing the relaxation of the nuclear spin magnetization in $^{15}N_2$. The curves are the results of CT calculations for the LJ(12,6,8) (solid curve) and the LJ(12,6) (dashed curve) potential energy surfaces, while the symbols represent the experimental results obtained in Refs. 15 and 16.

of an earlier potential surface[8] are in quite reasonable agreement with experiment. The second interaction virial coefficients obtained from this new LJ(12,6,8) potential surface can be considered to be in good agreement with experiment, in marked contrast to the rather poor agreement obtained for the original LJ(12,6) potential surface (see Table II). Further, the centers of gravity of the hyperfine structure microwave lines calculated from the new surface are in excellent agreement with experiment (recall that only the 1–2, 2–3 transitions for the $^{14}N_2$–^{86}Kr complex were involved in the fitting procedure), in all cases to better than $\pm 0.3\%$. This may be contrasted with the comparable level of agreement of $\pm 2\%$ for the LJ(12,6) potential surface. Neither the diffusion coefficients calculated from the LJ(12,6,8) potential surface nor those calculated from the original LJ(12,6) potential surface always lie within the somewhat optimistic reported experimental error bars. However, the experimental values from the different laboratories tend to disagree by about the same amount from one another as from the present calculations. It is thus not entirely clear which experimental values should be treated as definitive. The agreement between the mixture shear viscosity calculated from the LJ(12,6,8) potential surface and the experimental data of Ref. 12 is satisfactory, though it could be better, since the calculated values do not lie systematically within the (rather stringent) experimental error bars of $\pm 0.5\%$. The agreement between the thermal conductivity calculated from the present potential and that measured at 300.65 K is not particularly good; it does, however, provide an improvement over the level of agreement found for the original LJ(12,6) potential surface. Finally, agreement between the NMR relaxation cross sections calculated from the LJ(12,6,8) potential surface and those obtained from experiment is good, though not quite as good as that found for the LJ(12,6) potential surface. This indicates that the anisotropy parameter b_2 could have been made a little smaller.

ACKNOWLEDGMENTS

This work has been supported in part by a NSERC of Canada grant in aid of research and by the National Science Foundation (Grant No. CHE92-10790). We are grateful to E. E. Hanson for the calculation of second-approximation correction factors, and to Professor R. J. Le Roy for helpful comments on this paper.

[1] R. Shafer and R. G. Gordon, J. Chem. Phys. **58**, 5422 (1973).
[2] W. R. Rodwell and G. Scoles, J. Phys. Chem. **86**, 1053 (1982).
[3] K. T. Tang and J. P. Toennies, J. Chem. Phys. **80**, 3726 (1984).
[4] (a) R. J. Le Roy and J. van Kranendonk, J. Chem. Phys. **61**, 4750 (1974); (b) R. J. Le Roy and J. S. Carley, Adv. Chem. Phys. **42**, 353 (1980).
[5] R. J. Le Roy and J. M. Hutson, J. Chem. Phys. **86**, 837 (1986).
[6] H. L. Williams, K. Szalewicz, B. Jeziorski, R. Moszynski, and S. Rybak, J. Chem. Phys. **98**, 1279 (1993).
[7] J. M. Hutson, J. Chem. Phys. **96**, 4237, 6752 (1992); J. Phys. Chem. **96**, 4237 (1992).
[8] G. Rotzoll, Chem. Phys. Lett. **88**, 179 (1982).
[9] M. Faubel, K. H. Kohl, J. P. Toennies, K. T. Tang, and Y. Y. Yang, Faraday Discuss. Chem. Soc. **73**, 205 (1982); M. Faubel, J. Chem. Phys. **81**, 5559 (1984); M. Faubel, K. H. Kohl, and J. P. Toennies, *ibid*. **73**, 2506 (1980).
[10] L. Beneventi, P. Casavecchia, and G. G. Volpi, J. Chem. Phys. **70**, 541 (1986).
[11] See, for example, J. H. Dymond and E. B. Smith, *The Virial Coefficient of Pure Gases and Mixtures* (Clarendon, Oxford, 1980).
[12] J. M. Hellemans, J. Kestin, and S. T. Ro, J. Chem. Phys. **57**, 4038 (1972).
[13] R. D. Fleeter, J. Kestin, R. Paul, and W. A. Wakeham, Physica A **108**, 371 (1981).
[14] R. A. J. Keijser, K. D. van den Hout, and H. F. P. Knaap, Physica **108**, 371 (1981); R. J. van den Oord, W. Mischke, and J. J. M. Beenakker, Physica A **139**, 41 (1986).
[15] C. J. Jameson, A. K. Jameson, and N. C. Smith, J. Chem. Phys. **86**, 6833 (1987).
[16] C. J. Jameson, A. K. Jameson, and M. A. ter Horst, J. Chem. Phys. **95**, 5799 (1991).
[17] A. R. W. McKellar, J. Chem. Phys. **88**, 4190 (1988).
[18] W. Jäger and M. C. L. Gerry, Chem. Phys. Lett. **96**, 274 (1992).
[19] W. Jäger, Y. Xu, N. Heineking, and M. C. L. Gerry, J. Chem. Phys. **99**, 7510 (1993).
[20] M. S. Bowers, K. T. Tang, and J. P. Toennies, J. Chem. Phys. **88**, 5465 (1988).
[21] L. Beneventi, P. Casavecchia, G. G. Volpi, C. C. K. Wong, F. R. W. McCourt, G. C. Corey, and D. Lemoine, J. Chem. Phys. **95**, 5827 (1991).
[22] L. Beneventi, P. Casavecchia, F. Vecchiocattivi, G. G. Volpi, D. Lemoine, and M. H. Alexander, J. Chem. Phys. **89**, 3505 (1988).
[23] L. Beneventi, P. Casavecchia, G. G. Volpi, C. C. K. Wong, and F. R. W. McCourt, J. Chem. Phys. **98**, 7926 (1993).
[24] F. R. W. McCourt, J. J. M. Beenakker, W. E. Köhler, and I. Kuščer, *Nonequilibrium Phenomena in Polyatomic Gases. Vol. 1. Dilute Gases* (Clarendon, Oxford, 1990).
[25] W. Jäger, M. C. L. Gerry, C. Bissonnette, and F. R. W. McCourt, Faraday Discuss Chem. Soc. **97**, 105 (1994).
[26] R. T Pack, Chem. Phys. Lett. **55**, 197 (1978).
[27] C. Nyeland and J. P. Toennies, Chem. Phys. **122**, 337 (1988).
[28] H. Hettema, P. E. S. Wormer, and A. J. Thakkar, Mol. Phys. **80**, 533 (1993); A. J. Thakkar, H. Hettema, and P. E. S. Wormer, J. Chem. Phys. **97**, 3252 (1992).
[29] (a) R. Ahlrichs, R. Penco, and G. Scoles, Chem. Phys. **19**, 119 (1977); (b) K. T. Tang and J. P. Toennies, J. Chem. Phys. **68**, 5501 (1978).
[30] F. R. W. McCourt and L. V. Bissonnette (unpublished).
[31] M. A. ter Horst, Ph.D. thesis, University of Illinois at Chicago, unpublished; see also M. A. ter Horst and C. J. Jameson, J. Chem. Phys. (in press).
[32] J. Brewer, Determination of Mixed Virial Coefficients, Tech. Report AADD 663448, AFOSR No. 67-2795 (Air Force Office of Scientific Research, Arlington VA, 1967).
[33] J. Tennyson, S. Miller, and C. R. Le Sueur, Comp. Phys. Commun. **75**, 339 (1993).
[34] F. R. W. McCourt, in *Status and Future Developments in Transport Properties*, NATO ASI Series C361, edited by W. A. Wakeham, A. S. Dickinson, F. R. W. McCourt, and V. Vesovic (Kluwer, Dordrecht, 1992), p. 117.
[35] R. D. Trengove and P. J. Dunlop, Physica A **115**, 339 (1982).
[36] A. S. M. Wahby, Physica C **145**, 78 (1987).
[37] T. R. Marrero and E. A. Mason, J. Phys. Chem. Ref. Data **1**, 3 (1972).
[38] G. C. Maitland, M. Rigby, E. B. Smith, and W. A. Wakeham, *Intermolecular Forces: Their Origin and Determination* (Clarendon, Oxford, 1981).
[39] R. A. Aziz and M. J. Slaman, Mol. Phys. **58**, 679 (1986).
[40] E. L. Heck and A. S. Dickinson, Mol. Phys. **81**, 1325 (1994).
[41] A. van der Avoird, P. E. S. Wormer, and A. P. J. Jansen, J. Chem. Phys. **84**, 1629 (1986).
[42] E. L. Heck, A. S. Dickinson, and V. Vesovic, Mol. Phys. **83**, 907 (1994).
[43] C. Lemaire, R. L. Armstrong, and F. R. McCourt, J. Chem. Phys. **81**, 5275 (1984); R. S. Wagner, R. L. Armstrong, C. Lemaire, and F. R. McCourt, *ibid*. **84**, 1137 (1986); C. Lemaire, R. L. Armstrong, and F. R. McCourt, *ibid*. **87**, 6499 (1987).
[44] J. A. Barker and A. Pompe, Austr. J. Chem. **21**, 1683 (1968).
[45] A. J. C. Varandas, Adv. Chem. Phys. **74**, 255 (1988).